JOURNAL OF SPACECRAFT AND ROCKETS
Vol. 29, No. 6, November–December 1992

Electron Emission from a Hollow Cathode-Based Plasma Contactor

John D. Williams*
Hughes Research Laboratories, Malibu, California 90265
and
Paul J. Wilbur†
Colorado State University, Fort Collins, Colorado 80523

Emissive and Langmuir probes were used to measure plasma potential profiles, plasma densities, electron energy distributions, and plasma noise levels near a hollow cathode-based plasma contactor emitting electrons. The effects of electron emission current (0.1 to 1.5 A) and contactor flowrate [2 to 10 sccm (xenon)] on these data are examined. Retarding potential analyzer (RPA) measurements showing that high-energy ions generally stream from a contactor along with the electrons being emitted are presented and a mechanism by which these ions are produced is postulated. This mechanism, which involves a high rate of ionization induced between electrons and atoms flowing together from the hollow cathode orifice, results in a region of high positive space charge and high positive potential. Langmuir and RPA probe data suggest that both electrons and ions expand spherically from this potential hill region. In addition to experimental observations, a simple one-dimensional model which describes the electron emission process and predicts the phenomena just mentioned is presented and is shown to agree qualitatively with experimental observations.

Nomenclature

E = electron energy, eV
e = magnitude of electronic charge, 1.60×10^{-19} C
$F(E)$ = electron energy distribution function (normalized)
J_{CD} = contactor discharge current, A
J_{CE} = electron current emitted by contactor, A
J_p = ion current at r_e due to ions produced between r_e and r_B which flows from the potential hill region to the cathode, A
J_{SD} = simulator discharge current, A
J_{SE} = electron current collected by simulator, A
J_{SF} = simulator filament cathode heating current, A
J_{str} = streaming (or high-energy) electron current flowing to the Langmuir probe when it is held at plasma potential, A
J_+ = ion current at r_A due to ions produced between r_B and r_A which flow from the potential hill region to the downstream boundary, A
j_+ = current density of high-energy ions flowing from the vicinity of the contactor to regions downstream of it, A-m^{-2}
k = Boltzmann's constant, 1.38×10^{-23} J-K^{-1}
$\dot{m}_c$ = flowrate of neutrals supplied to contactor [sccm (Xe)—standard cubic centimeters per minute]
m_e = mass of electron, 9.11×10^{-31} kg
m_p = mass of ion, xenon: 2.18×10^{25} kg
$\dot{n}$ = neutral atom supply rate (from hollow cathode), s^{-1}
n_e = electron density, m^{-3}
n_o = neutral atom density, m^{-3}
n_p = density of ions on the cathode side of the potential hill (i.e., those that flow toward the cathode), m^{-3}
n_+ = density of ions on the downstream side of the potential hill (i.e., those that flow toward the downstream boundary) m^{-3}
P_o = ambient pressure measured far from the hollow cathode, Pa
$R(r)$ = volumetric production rate of ions at radius r, s^{-1}-m^{-3}
r = radius measured from the hollow cathode orifice, m
r_1 = radius measured from the hollow cathode (used as an integration variable), m
r_A = radial position of the spherical shell at the downstream boundary (i.e., at the base of the potential hill), m
r_B = radial position of the potential hill peak (or crest), m
r_e = radial position of the spherical shell boundary from which electrons are supplied, m
T_o = neutral atom temperature measured far from the hollow cathode, K
V = potential measured with respect to (wrt) the contactor cathode, V
V_A = potential at r_A, downstream boundary potential (wrt contactor cathode), V
V_B = potential at r_B, crest potential (wrt contactor cathode), V
V_C = bias supply voltage (wrt contactor cathode), V
V_{CD} = contactor discharge voltage, (wrt contactor cathode), V
V_{SD} = simulator discharge voltage (wrt simulator cathode),
v_e = electron velocity, m-s^{-1}
v_{oc} = velocity of neutrals flowing from the hollow cathode, m-s^{-1}
Z = axial position measured from the contactor cathode along the tank/contactor centerline, m
ϵ_o = permittivity of free space, 8.85×10^{-12} F-m^{-1}
ψ = solid angle of the spherical sector through which electron emission occurs, sr
ψ_o = solid angle of the spherical sector through which neutral atoms expand as they exit the orifice of the hollow cathode, sr
σ_+ = electron/neutral atom ionization cross-section, m^2

Introduction

SEVERAL experimental[1-3] and theoretical studies[4-6] have addressed the problem of controlling spacecraft electric potential with respect to an adjacent environment using

---

Received Sept. 10, 1991; revision received May 12, 1992; accepted for publication May 12, 1992. Copyright © 1992 by John D. Williams and Paul J. Wilbur. Published by the American Institute of Aeronautics and Astronautics, Inc., with permission.

*Member of the Technical Staff, Plasma Physics Laboratory. Member AIAA.

†Professor, Department of Mechanical Engineering. Member AIAA.

plasma producing devices. These studies involved electrodynamic tether applications in which the plasma producing devices provide relatively high current capacity "contacts" to space plasmas at each end of the tether. Most of this work concentrated on the processes that occur at the positively biased "plasma contactor" (i.e., the one collecting electrons from and emitting ions to the space plasma); and little attention was given to the negatively biased contactor that emits electrons. This study addresses this deficiency by focusing on the processes that occur near a plasma contactor emitting electrons to a simulated space plasma in a laboratory environment. The plasma contactor used in these experiments is a hollow cathode—a device derived from ion thruster neutralization applications. The hollow cathode plasma source is particularly well suited to charge control applications because of its robust construction and long lifetime characteristics, high electron emission current capabilities (in excess of 60 A),[7] and capacity to produce a cool, neutral plasma.

Observations of the particles coming from a contactor emitting electrons made using a retarding potential analyzer (RPA) show that relatively high-energy ions stream away along with the electrons being emitted. A mechanism is postulated in this study that could explain this observation. An important part of the mechanism is the high rate of ionization that occurs when atoms and electrons are expelled simultaneously through a small orifice as they are in a hollow cathode discharge.[7,8] A similar mechanism for the creation of high-energy ions has also been proposed by investigators[9,10] studying various electric arcs. A plasma contactor operating in this manner (emitting both ions and electrons) should be well suited to spacecraft charging control because small changes in the potential difference between the spacecraft and the ambient plasma should cause the currents associated with the ion and electron flow between the contactor and space plasma to be altered. This would be expected in turn to facilitate the changes in current required to prevent the spacecraft from becoming either substantially positive or negative of the plasma surrounding it in a variety of spacecraft charging situations. This work describes recent experimental results obtained on a hollow cathode emitting a net electron current to a surrounding ambient plasma and presents a first order, one-dimensional model of the process.

Apparatus and Procedure

To study the electron emission process, the apparatus shown schematically in Fig. 1 was constructed. Physically, this apparatus consists of two plasma producing devices. The one shown at the right and labeled "simulator" generates a simulated ionospheric plasma. The other device, shown on the left and labeled plasma contactor, is the focus of this study and is biased negative relative to the ambient plasma to induce electron emission. Also shown are the power supplies and instrumentation needed to sustain and measure the characteristics of the plasmas produced. The simulator and contactor devices are separated by 2.7 m and are located within a 1.2-m-diam by 5.3-m-long vacuum chamber. The contactor utilizes a 6.4-mm-diam hollow cathode that contains an electron emitting insert fabricated by rolling 0.013-mm-thick tantalum foil into the shape of a hollow cylinder and treating it with a low work function coating [containing a double carbonate ($BaCO_3$, $SrCO_3$)]. An orifice plate with a 1.0-mm-diam orifice caps the downstream end of the hollow cathode tube. The contactor anode is a 12-cm-diam stainless-steel plate with a 1 cm o.d./5 mm i.d. tantalum insert near its center. The tantalum anode insert is aligned with the hollow cathode orifice and positioned ~ 2 mm downstream of it.

Physically, the simulator resembles a ring-cusp ion source used in ion thruster applications.[11] Plasma is generated within it by collisions between high-energy discharge electrons and neutral atoms. To increase the efficiency of this process, magnetic fields are used to shield anode surfaces and chamber walls against direct loss of discharge electrons. The ring-cusp magnetic field used in the simulator is induced by samarium cobalt permanent magnets. To ensure good coupling between the plasma produced within the source and the ambient plasma region, the device was operated without extraction grids. The simulator is equipped with a tungsten wire cathode which is stretched diagonally across the 9-cm-diam open end of the source. When it is heated to thermionic temperatures, it emits electrons that are eventually collected at the simulator body, which serves as the anode for this device as Fig. 1b suggests. For most of the experimental results presented in this study, the simulator discharge current and voltage were set at 0.5 A and 40 V, respectively, and the simulator flowrate was set at 2.7 sccm (Xe).

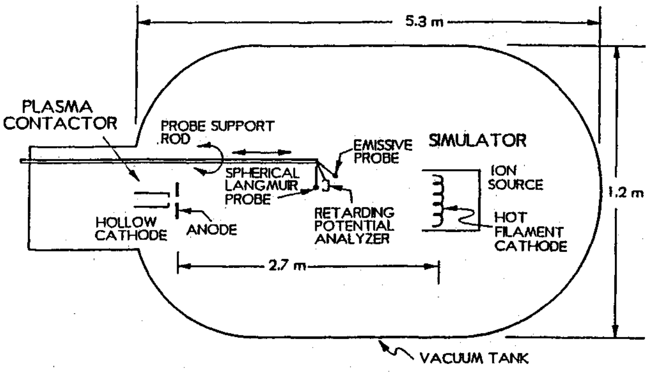

a) Mechanical schematic

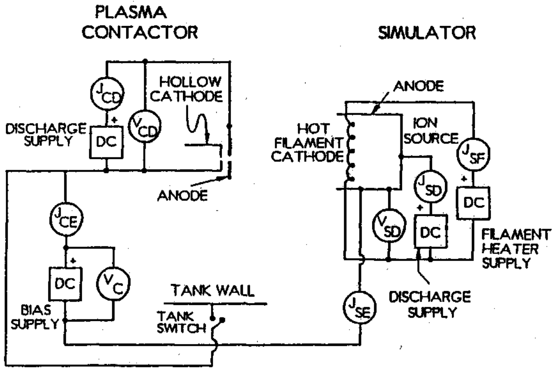

b) Electrical schematic

Fig. 1 Experimental apparatus.

Typical tests were conducted by heating the contactor hollow cathode to a temperature where significant thermionic electron emission could occur from the insert (~ 1300 K), establishing a high expellant (xenon) flowrate through it, and biasing its anode positive using the discharge supply to initiate a cathode-to-anode discharge. Next, the desired contactor flowrate and discharge current were established; the contactor was biased relative to the simulator using the bias power supply; and voltage, current, and probing instrument data were collected. The voltages and currents measured during typical tests are designated by the symbols shown within the circles in Fig. 1b and defined in the nomenclature list. These quantities include the contactor and simulator discharge currents and voltages, the bias voltage between the contactor and simulator, and the contactor and simulator electron emission currents.

The tank bias switch shown in Fig. 1b was installed so that the vacuum tank could be allowed to float relative to the contactor-simulator system or could be connected to the contactor cathode. Experimental results were typically not affected by the switch position and, consequently, it was left closed for the tests described here. The plasma environment produced between the contactor and the simulator was probed using the various instruments shown in Fig. 1a. They include an emissive probe, a Langmuir probe, and a retarding potential analyzer (RPA). The RPA consists of a cylindrical Faraday cage with an orifice plate at one end—the orifice hole diameter of 3 mm was selected to be smaller than the Debye length of the plasma in which it is typically used. The Faraday cage was held about 40 V below the potential of the plasma in which it was immersed. The probe is operated by first sighting the RPA orifice at the plasma contactor and then recording the ion current to the probe collector as its voltage is swept from 10 V below contactor cathode potential to about 100 V above it. The details of the current/voltage traces obtained and their analysis and interpretation are discussed in Refs. 7 and 12.

The plasma conditions associated with the experiments described herein differ from those a satellite would see in low Earth orbit (LEO). It was not possible to match the LEO conditions in part because the electron emission current significantly affected the plasma density throughout the vacuum chamber in our experiments. This is unfortunate because it prevented a detailed study of the effects of background plasma density on phenomena that will occur near a contactor in LEO. Furthermore, both the background plasma density ($\sim 10^7$–10^8 cm^{-3}) and electron temperature (2–6 eV) were higher than those in LEO. Accurate simulation of the LEO environment is difficult to realize in a vacuum chamber not only because of emission-current-induced effects, but also because unrealistically large chambers would be needed to prevent wall effects from dominating the tests. Although these experiments were not conducted at LEO conditions, they do facilitate an understanding of contactor phenomena. They also provide data for validation of theoretical models which can be used to predict plasma contactor performance under LEO conditions.

Experimental Observations

Some of the phenomena observed in ground-based studies of the process of electron flow from a hollow cathode-based plasma contactor to a low-density ambient plasma can be explained using the typical plasma potential profile shown in Fig. 2. In this case, the contactor cathode, at zero potential and zero axial position, was emitting 61 mA of electrons into an ambient background plasma located about 1 m downstream of the contactor. A noteworthy feature of this potential profile is the hill structure that develops immediately downstream of the contactor. It is postulated that this potential hill develops because the densities of both neutrals and electrons (with sufficient energy to ionize them) are high near the contactor. Under this condition, electrons that cause the ionization and the electrons produced would typically be expected to have substantial kinetic energies after the ionization event, and they would be expected to leave the region quickly. However, the more massive ions would be left behind, thereby creating a region in which the ion density would tend to be greater than the electron density. This positive-space-charge density region would induce a potential hill like the one shown in Fig. 2. It should be noted that the plasma potential data of Fig. 2 were obtained using a floating emissive probe, and these probes indicate potentials that fall progressively further below true plasma potential as they are moved into higher density plasmas.[13] Because plasma density is greatest at the hollow cathode orifice, the emissive probe probably indicates potentials that fall below actual values as the cathode is approached at $Z = 0$. Hence, it is possible that the true crest of the hill is higher and located at a different axial position than the one indicated in Fig. 2.

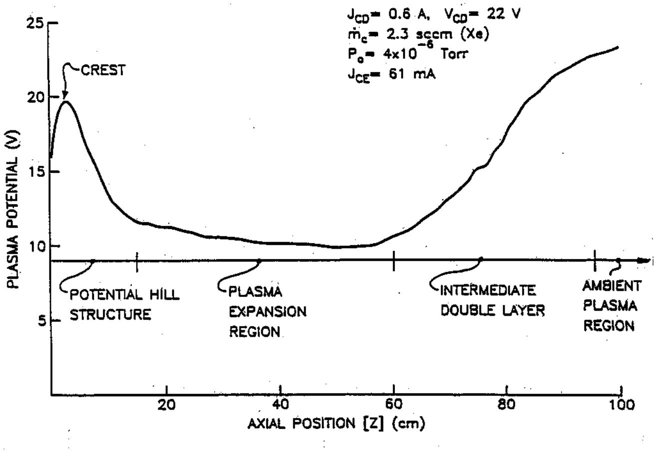

Fig. 2 Plasma potential profile on the contactor/vacuum tank centerline (contactor emitting electrons).

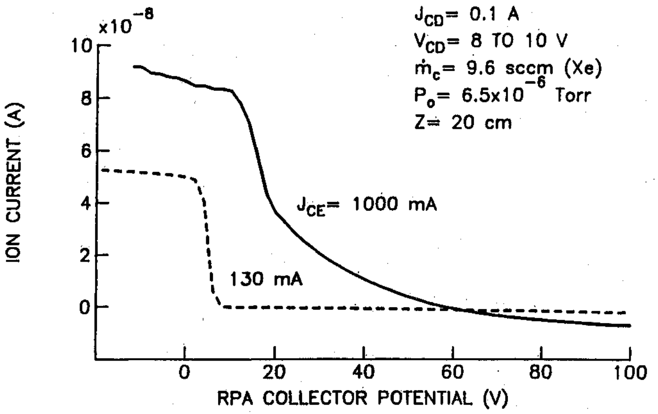

a) Current/voltage traces

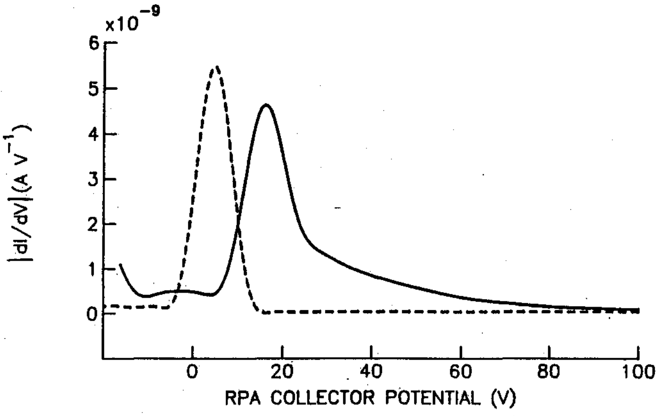

b) Derivatives of current/voltage traces

Fig. 3 Retarding potential analyzer data measured in the expanding plasma region (high contactor flowrate condition).

Downstream of the potential hill, Fig. 2 shows that the plasma potential is relatively constant from 15 to 60 cm. This region is called the plasma expansion region because the plasma density decreases in proportion to Z^{-2} there and this in turn suggests a region of spherical plasma expansion.[1] Generally, it appears that the plasma overexpands in this region. This is demonstrated by Langmuir probe data[1] which show that the plasma density at the downstream end of the plasma expansion region is below that of the ambient plasma region (the region of constant plasma potential extending beyond 100 cm in Fig. 2). It appears that the intermediate double layer (shown between 60 and 100 cm) enables accommodation of this difference in plasma densities. These phenomena and double layers in general are discussed in more detail by Hershkowitz[14] and the references he cites. The criteria that determine the location, geometry, and size of the intermediate double layer probably depend upon the ion creation and loss rates in the ambient and expanding plasma regions, the ion and electron current densities, and interactions with the vacuum test facility walls. However, the details of its characteristics have not been investigated in this study.

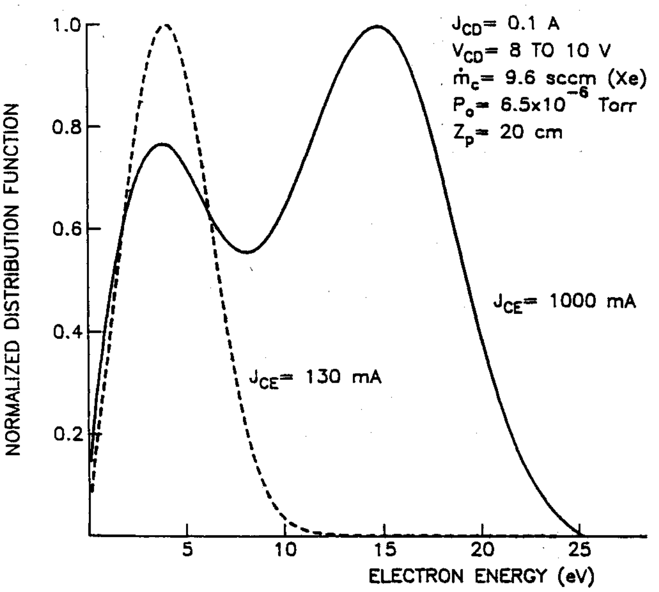

Fig. 4 Electron energy distributions measured in the expanding plasma region (high contactor flowrate condition).

A relatively low flowrate [2.3 sccm (Xe)] and emission current (61 mA) were selected for the measurements of Fig. 2 because these operating conditions yielded a sufficiently low plasma density near the cathode which enabled the emissive probe to detect the potential hill. As flowrate and/or electron emission current were increased, the potential hill (as detected by the emissive probe) began to disappear. To determine if this was due to emissive probe inadequacy or an actual reduction in the height of the potential hill, an RPA was positioned in the plasma expansion region and used to measure the energy characteristics of the ions coming from the vicinity of the contactor. Two typical RPA traces (recorded with the RPA positioned at $Z = 20$ cm and sighted at the contactor cathode) along with their corresponding derivatives are shown in Fig. 3. These data were obtained with the contactor operating at a high flowrate [9.6 sccm (Xe)], where emissive probe measurements showed no evidence of potential hills at either the 130 or 1000 mA electron emission levels. The RPA curve and corresponding derivative for the high emission current case ($J_{CE} = 1000$ mA) indicate that two groups of ions are present. The first group induces the peak occurring near 15 V in the lower plot and represents low-energy, thermal ions present in the expanding plasma. The second group which exhibits a greater energy spread is present as the tail on the solid curve extending from 20 to 100 V (Fig. 3b). It is postulated that the high-energy ions associated with this tail are created on a potential hill located near the contactor cathode and that they flow from there to the RPA where they are detected. The RPA data corresponding to contactor operation at a low electron emission current of 130 mA displays only one low-energy group of ions. Hence, it is concluded that the potential hill is still present at the 1000-mA emission current operating condition and that it is not present at the 130-mA one.

There are other differences between the plasmas measured in the expanding plasma region at 130- and 1000-mA emission currents and one of these, the difference in electron energy distribution functions sensed by a Langmuir probe, is illustrated in Fig. 4. At a high emission current, the solid curve suggests that two electron groups exist. One group, associated with the lower energy peak, probably represents the thermal electrons present in the expanding plasma. The other, higher energy group contains electrons that have been accelerated from the contactor cathode through the potential hill region and into the expanding plasma without experiencing many energy dissipating collisions. The electron distribution function corresponding to the low emission current condition ($J_{CE} = 130$ mA) indicates, on the other hand, only one, low-energy group of electrons is present. Thus, Figs. 3 and 4 show that both ions and electrons in the expanding plasma region exhibit distribution functions that have thermal and high-energy components at a high emission current, while only the thermal component is present at a lower electron emission current. Note that the electron energy distribution functions shown in Fig. 4 have been normalized with respect to their maxima. They were computed from the second derivatives of spherical Langmuir probe traces recorded digitally using a Keithley 617 programmable electrometer and plasma potential data measured using the emissive probe. The derivatives were obtained by finding the discrete Fourier series representation of the Langmuir probe trace, solving for the analytical derivative of this series, and applying a convergence filter.[15] The convergence filter artificially smooths the data and tends to spread out quickly varying features of the Langmuir probe trace. Smoothing errors introduced by the data-reduction procedure and plasma potential measurement errors yield distribution functions (Fig. 4) that reflect only the qualitative differences between the plasmas observed at the 130- and 1000-mA operating conditions.

It is also of interest to examine the effect of electron emission current on the axial profiles of the high-energy ion current density measured using the RPA and the high-energy (or streaming) electron current measured using the Langmuir probe. These profiles have been measured over a range of electron emission currents and the results are shown in Fig. 5. The data in this figure correspond to a lower flowrate [4.1 sccm (Xe)] than those of Figs. 3 and 4. At this lower flowrate, high-energy ions were detected flowing from the contactor at all four of the electron emission current levels shown (i.e., at

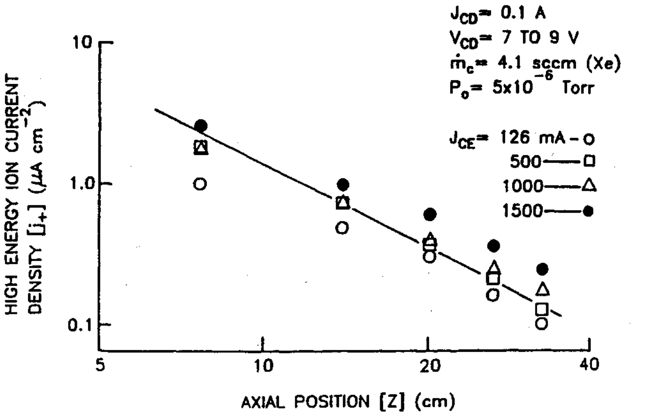

a) Effect of electron emission current on high energy ion current density profiles

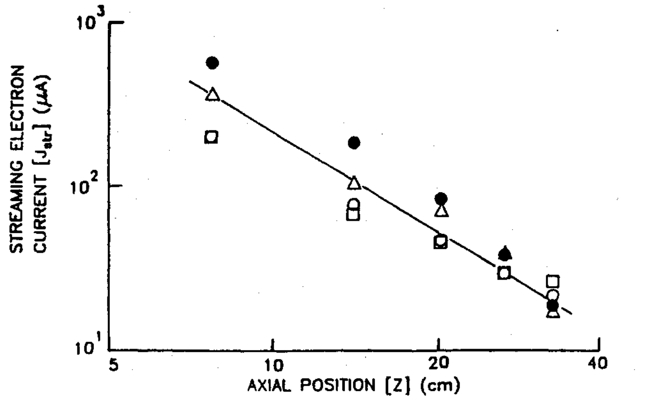

b) Effect of electron emission current on streaming electron current profiles (streaming current flow to a 3.1 mm diam, spherical Langmuir probe)

Fig. 5 Experimental observations suggesting spherical expansion in the region downstream of the potential hill.

J_{CE} = 126, 500, 1000, and 1500 mA). The lines drawn on the two plots shown in Fig. 5 correspond to an inverse-square dependence with axial position.

The high-energy ion current density is also shown to follow the inverse-square dependence (Fig. 5a) and this suggests that these ions are also expanding spherically from their point of creation. In addition, the streaming electron current flowing to the Langmuir probe also decreases as the inverse square of distance as shown in Fig. 5b. Figure 5b shows that the streaming electron current begins to decrease faster than with inverse distance squared at large values of axial position and high electron emission currents. This may be occurring either because the streaming electrons are being thermalized or their presence is being masked by thermal electrons. In general, however, the data presented in Fig. 5 suggest ions and electrons are expanding from what is essentially a point source near the potential hill. Because of this expansion behavior, the region immediately downstream of the hill region is called the plasma expansion region.

Both the high-energy ion and directed electron populations present in the plasma expansion region can induce instabilities as they pass through the thermal plasma there and this can cause the plasma to be noisy (or turbulent). A coarse measure of the turbulent intensity (the fraction of the energy in the plasma expansion region that is in the form of turbulent electrostatic fluctuations) is the square of the ratio of the rms density fluctuations to the mean plasma density. This density ratio can be measured qualitatively by monitoring the current to a Langmuir probe when it is held near plasma potential and recording the rms noise amplitude/mean current ratio. Figure 6 shows rms-to-mean current ratio vs axial position data measured at the operating conditions of Figs. 3 and 4. The data for the 1000 mA operating condition suggest that the plasma is very noisy near the plasma contactor [turbulent intensity ~ $(0.32)^2 = 10\%$] and less noisy (~ 2%) further downstream. The opposite trend is indicated for the 130-mA operating condition. The noise levels at 33 cm are shown to be comparable thereby suggesting that phenomena occurring in the ambient plasma region determine the noise level at axial positions greater than about 30 cm.

Theoretical Development

To gain some understanding of the potential hills that have been measured at low emission currents and postulated at higher ones, a simple model of the electron emission process has been developed. Figure 7 shows a sketch of the postulated physical arrangement in spherical geometry and a hypothetical potential profile. The power needed to sustain the hill is assumed to come from the electron emission current J_{CE} flowing from the hollow cathode through the potential hill to a downstream boundary. As these electrons leave the electron source surface, they are accelerated up the potential hill and they gain sufficient energy to ionize neutral atoms. The resulting ions will flow down the hill from the point where they were produced. Ions produced to the left of the crest potential shown in Fig. 7 will flow to the cathode and those produced to the right of it will flow through the downstream boundary. The electrons, which accelerate to the crest and then decelerate after they pass it, will still have substantial kinetic energies as they pass the downstream boundary. They represent the streaming electrons mentioned in conjunction with Fig. 5.

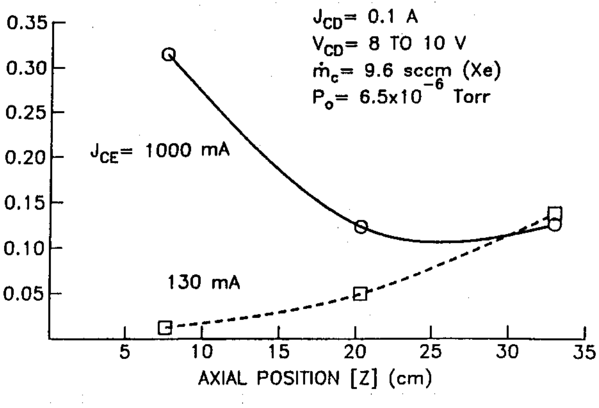

Fig. 6 Langmuir probe noise levels at high and low electron emission currents (high contactor flowrate condition).

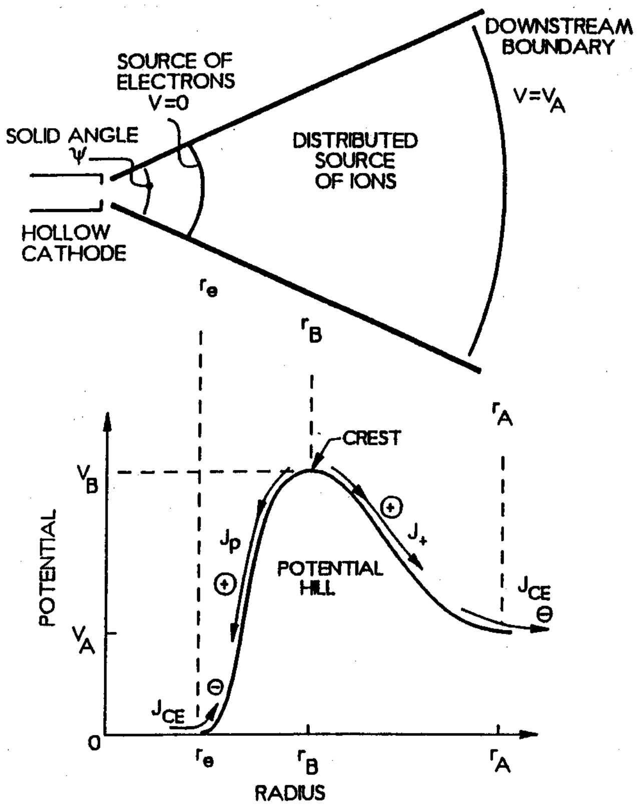

Fig. 7 Spherical model diagram of the electron emission process.

The approach used to model this problem will be to write equations that describe the electron and ion densities throughout the region between the electron source and the downstream boundary and then apply Poisson's equation to solve for the associated potential profile. Because the electron and ion densities depend upon the potential profile, however, an iterative solution technique must be applied to accomplish this and obtain the steady-state, self-consistent solution for the density and potential profiles. This model of the electron emission process will be presented in terms of two sets of equations. One set will pertain to radial locations between the cathode and the potential peak (i.e., on the cathode side of the potential hill). The other set will pertain to radial locations between the potential hill and the downstream boundary (i.e., on the downstream boundary side).

The Cathode Side ($r_e < r < r_B$)

The electron density at any point in this region can be described approximately by assuming conservation of electron energy and current, i.e.

$$\tfrac{1}{2} m_e [v_e(r)]^2 = eV(r) \tag{1}$$

and

$$J_{CE} = e n_e(r) \psi r^2 v_e(r) \tag{2}$$

Combining these equations and solving for the electron density gives

$$n_e(r) = \frac{J_{CE}}{e\psi r^2}\sqrt{\frac{m_e}{2eV(r)}} \tag{3}$$

This expression is only approximately correct because it ignores both electrons which are produced in ionization events and the effects of energy removal from the electron group due to ionization and other inelastic collisions. Neglecting these effects to make the problem more tractable limits its direct applicability to the case where the inelastic collision rate expressed as a current is small compared to the electron emission current. It is assumed that some mechanism for removing low-energy electrons produced via ionization from the potential hill region is active. Although this mechanism is not defined, it is noted that the current of these electrons should be small so a negligible fraction of the kinetic power in the streaming electrons would be required to remove them through elastic collisions.

The rate of ion generation per unit volume $[R(r)]$ at radius r is given by

$$R(r) = n_e(r) n_o(r) \sigma_+ (v_e) v_e(r) \tag{4}$$

The ionization cross-sections of Rapp and Englander-Golden[16] were used to calculate ion generation rates. In addition, the neutral atom density n_o appearing in this equation was modeled as the sum of the neutral densities due to the neutral flow from the hollow cathode (assumed to expand spherically from the orifice) and the background neutral density in the vacuum environment of the test. Specifically, the density n_o at radius r was approximated by

$$n_o(r) = \frac{\dot{n}}{\psi_o r^2 v_{oc}} + \frac{P_o}{kT_o} \tag{5}$$

The density of ions at a radius r is determined by summing the contributions of all ions produced at radii of greater potential. Each of these ions will be accelerated from their point of creation r_1 to the radius of interest r. Hence, the contribution to the density of ions at a radial location r (for the region $r_e < r < r_B$) due to ions generated with a negligible initial velocity in a differential volume near r_1 is

$$\mathrm{d}n_p(r) = r^{-2} \frac{R(r_1) r_1^2 \, \mathrm{d}r_1}{v(r_1)} \tag{6}$$

and the velocity of the ions created at r_1 once they reach r is given by

$$v(r_1) = \sqrt{\frac{2e[V(r_1) - V(r)]}{m_p}} \tag{7}$$

The overall ion density at any radius r on the cathode side of the hill is now found by integrating the differential density $\mathrm{d}n_p$ from r to r_B. This yields

$$n_p(r) = r^{-2} \int_r^{r_B} \frac{R(r_1) r_1^2 \, \mathrm{d}r_1}{v(r_1)} \tag{8}$$

Combining Eqs. (3-8) and simplifying gives

$$n_p(r) = r^{-2} \frac{J_{\mathrm{CE}} \sqrt{m_p}}{\sqrt{2} \psi e^{3/2}} \int_r^{r_B} \left(\frac{\dot{n}}{\psi_o r_1^2 v_{oc}} + \frac{P_o}{kT_o} \right) \times [V(r_1) - V(r)]^{-1/2} \sigma_+ \, \mathrm{d}r_1 \tag{9}$$

The electron and ion densities determined using Eqs. (3) and (9) can now be combined with Poisson's equation to describe the variation in plasma potential on the cathode side of the potential hill. Assuming spherical symmetry, Poisson's equation is

$$\frac{\mathrm{d}^2 V}{\mathrm{d}r^2} + \frac{2}{r} \frac{\mathrm{d}V}{\mathrm{d}r} = \frac{e}{\epsilon_o} [n_e(r) - n_p(r)] \tag{10}$$

To utilize the equations just developed, it is necessary to develop the equations describing conditions on the opposite (downstream boundary) side of the potential hill so all of them can be solved simultaneously.

The Downstream Boundary Side ($r_B < r < r_A$)

Under the assumptions of this development, the equation that describes the electron density in the region between the potential crest and the downstream boundary is the same as the one developed for application upstream of the potential crest, namely Eq. (3). The ion density expression is obtained by repeating the logical sequence used to derive Eq. (9). It is found to differ from Eq. (9) only in the order of the integration; hence,

$$n_+(r) = r^{-2} \frac{J_{\mathrm{CE}} \sqrt{m_p}}{\sqrt{2} \psi e^{3/2}} \int_{r_B}^{r} \left(\frac{\dot{n}}{\psi_o r_1^2 v_{oc}} + \frac{P_o}{kT_o} \right) \times [V(r_1) - V(r)]^{-1/2} \sigma_+ \, \mathrm{d}r_1 \tag{11}$$

Note that Eq. (11) shows an inverse-square dependence with position and a linear dependence with emission current. This is in qualitative agreement with the functional dependencies indicated by the experimental data of Fig. 5a.

Equations (3), (9), (10), and (11) represent a relatively simple model of the electron emission process. They were solved by first dividing up the region r_e to r_A using closely and evenly spaced node points. Next, the derivatives in Eq. (10) were approximated using finite difference expressions. This allowed algebraic equations arranged in matrix form to be written for the potential at each node point. Electron and ion densities were then calculated at each node point using Eqs. (3), (9), and (11) and an initial estimate of the potential variation through the potential hill region. The procedure of solving for the densities and then the potentials at each node was repeated many times until the potential profile stabilized.

It should be noted that the solution procedure treats the electron source location r_e, the downstream boundary location r_A, the solid angles ψ and ψ_o, and the potential at the downstream boundary V_A as parameters. The electron source and downstream boundary locations are, however, not free parameters. The values of r_e and r_A are established physically by the requirement that the electric fields be zero at these locations (i.e., the space-charge limited condition applies). It was postulated that the other parameters, namely the downstream boundary potential V_A, and the solid angles ψ and ψ_o are influenced by such factors as the cathode orifice size, the anode configuration, and the plasma conditions beyond the downstream boundary and they were treated as free parameters. It is believed that an energy balance analysis could be used to find the downstream boundary potential, but this was not done in this preliminary study. To apply the model and compare its predictions to experimental observations, V_A was set at the experimentally measured potential in the expanding plasma region (typically measured at a radius of 20 cm) for each electron emission operating condition studied. The solid angles ψ and ψ_o were arbitrarily set to 2π (corresponding to hemispherical geometry). There are other parameters appearing in Eqs. (3), (9), (10), and (11) that are not determined explicitly through the analysis (e.g., P_o and T_o), but they were controlled during the experiment so unique values could be assigned to them.

Numerical Example

When Eqs. (3), (9), (10), and (11) were solved for the case of an emission current of 1 A and values of the parameters given in Table 1, the theoretical potential profile shown in Fig. 8a was computed. By forcing the electric fields at r_e and r_A to be zero, the electron source and downstream boundaries were found to be located at 4.6 and 14.4 mm, respectively. It is noted that the electric field shown at r_e in Fig. 8a is indeed near zero even though it does not appear to be so because of the

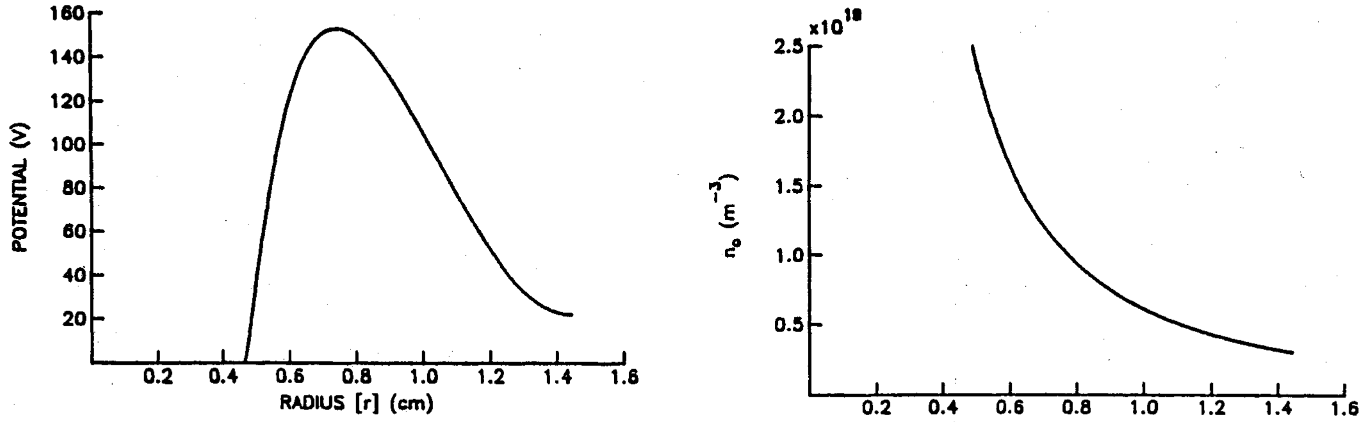

a) Potential profile

c) Neutral density

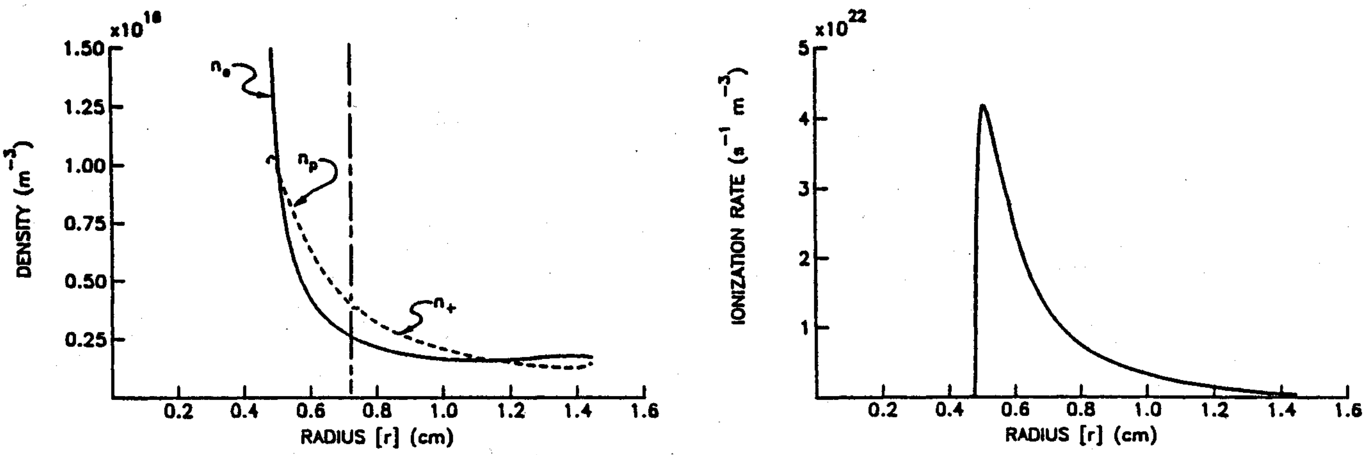

b) Charged particle densities

d) Ion production rate

Fig. 8 Typical computed electron emission results.

graphical scale. The crest potential of 153 V was located at 7.4 mm. This large potential was caused by the net positive (ion) charge density in the region between 5 and 11.5 mm as shown in Fig. 8b. The neutral atom density variation throughout the potential hill region is shown in Fig. 8c. When this information was combined with the data shown in Figs. 8a and 8b, the ion production rate per unit volume was calculated and it is plotted in Fig. 8d. By integrating the volumetric ion production rate over the entire volume of the potential hill region, the total ion current flowing from this region was calculated to be 4.10 mA. This ion current could be broken into components of 1.94 mA (J_+) and 2.16 mA (J_p) from the potential hill region to the downstream boundary and to the electron source boundary, respectively. These ion creation rates (expressed as currents) are small compared to the emission current. This suggests that the assumptions made in deriving this model are probably valid and that very little power should be required from the streaming electrons to remove low-energy electrons (resulting from inelastic collisions) from the potential hill as quickly as they are produced.

Comparison of Theory and Experiment

The procedures used to obtain the numerical results given in Table 1 and Fig. 8 were applied to obtain additional solutions over ranges of electron emission currents and flowrates. The effect of electron emission current and flowrate on the current density and maximum energy of ions flowing away from the hollow cathode discharge were also measured using the RPA described previously. The experimentally measured and numerically predicted effect of emission current on these quantities are compared in Fig. 9 under conditions where the RPA was positioned 20 cm downstream of the contactor. Figure 9a shows the high-energy ion current density increasing with electron emission current, at a smaller slope than the "theoretical" curve. The theoretical predictions of high-energy ion current density were made by first finding the ion current emitted from the potential hill region to the downstream boundary for the particular electron emission current as explained in the numerical example of Table 1 and Fig. 8. Next, this current was divided by the surface area at a radius of 20 cm (i.e., $\psi r^2 \approx 2\pi(20)^2$ cm$^2 \approx 2500$ cm^2) to obtain the current density at this location. Although the two curves shown in Fig. 9a do not coincide, the agreement between the experiment and numerical model is considered to be good considering the assumptions made in the model. Uncertainties in experimental conditions as well as in the ionization cross sections could easily cause the level of error indicated in Fig. 9a. It is noted that better agreement could be generated in this simple one-dimensional model by adjusting the solid angle ψ with each electron emission current. However, it is felt that two-dimensional (or possibly three-dimensional) effects probably deter-

Table 1 Numerical example data set

Inputs	Outputs
$J_{CE} = 1.0$ A	Fig. 8
$\dot{m}_c = 4.1$ sccm (Xe)	$J_+ = 1.94$ mA
(i.e., $\dot{n} = 1.72 \times 10^{18}$ s^{-1})	$J_p = 2.16$ mA
$P_o = 5.0 \times 10^{-6}$ Torr	$r_e = 4.6$ mm
(i.e., 6.7×10^{-4} Pa)	$r_B = 7.4$ mm
$T_o = 300$ K	$r_A = 14.4.$ mm
$v_{oc} = 458$ m-s^{-1}	$V_B = 153$ V
$\psi = 2\pi$	
$\psi_o = 2\pi$	
$V_A = 22$ V	

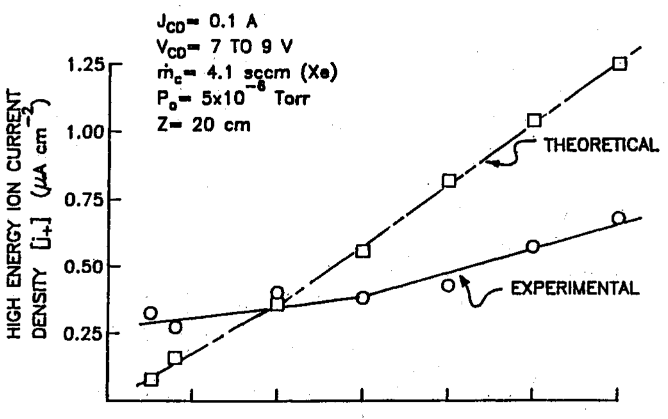

a) Ion current density

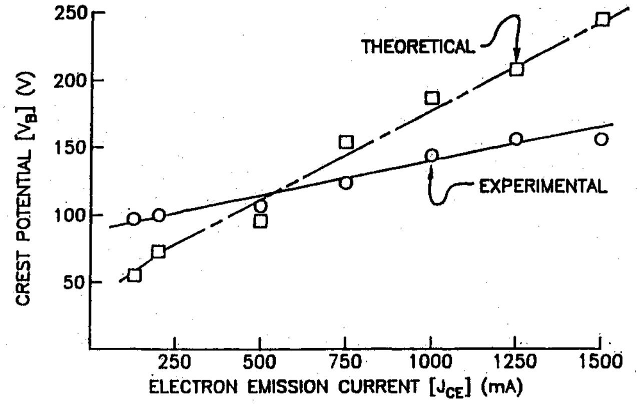

b) Crest potential

Fig. 9 Comparison of measured and computed effects of emission current.

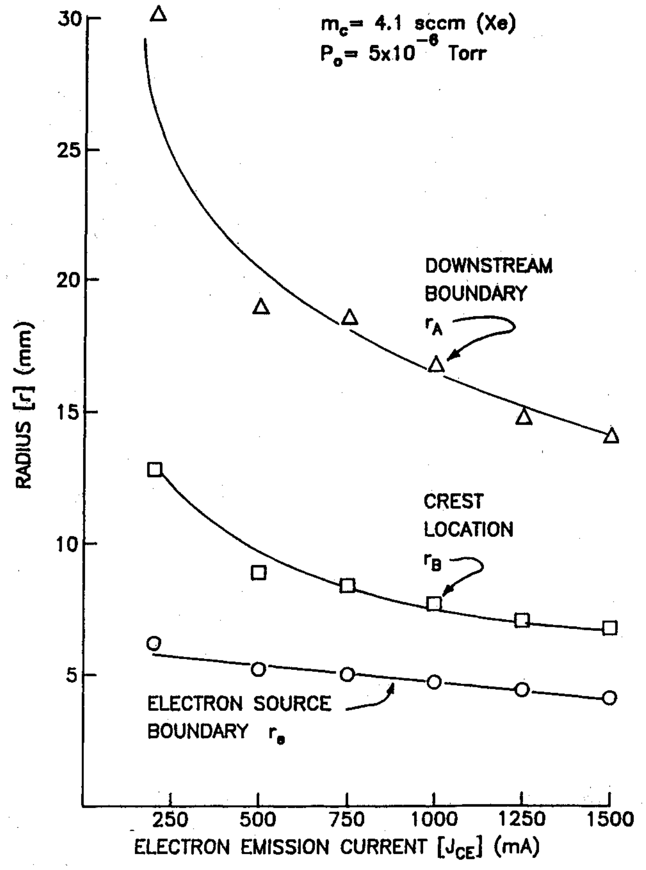

Fig. 10 Computed effects of electron emission current on the radii of electron source, crest, and downstream boundaries.

mine the subtle trends in the experimental data so attempts to adjust ψ to obtain better agreement cannot be justified.

Figure 9b contains a comparison of experimentally and theoretically determined crest potentials. Again, relatively good agreement and a similar trend for the crest potential to increase with electron emission current for both curves is shown. The computed positions of r_e, r_B, and r_A at the electron emission levels corresponding to Fig. 9 are shown in Fig. 10. The most notable trend in this figure is that larger values of r_A correspond to smaller values of electron emission current. Together with Fig. 9b, this suggests that not only are crest potentials greater at higher electron emission currents, but electric field strengths are also higher. Although it was generally not possible to measure the radii identified in Fig. 10 in the experiments, it is noted that the data of Fig. 2 (and visual estimations of the extent of the luminous region immediately downstream of the contactor) agree to first-order with the computed radii of Fig. 10.

The effect of contactor flowrate on the experimentally measured and numerically predicted high-energy ion current and crest potential are shown in Fig. 11. The theoretical predictions (triangular and solid circular data points) and experimental measurements (circular and square data points) of high-energy ion current density corresponding to the 130- and 1000-mA electron emission levels are shown to exhibit comparable magnitudes in Fig. 11a. The theoretical crest potential data for the 1000-mA condition shown in Fig. 11b also show good agreement with experiments, and the predicted and measured crest potentials show a similar trend (both decrease with flowrate). However, the predicted and measured crest potentials corresponding to the 130-mA condition do not show the same trends. Note that current density measurements made at an electron emission current of 130 mA (shown in Fig. 11a)

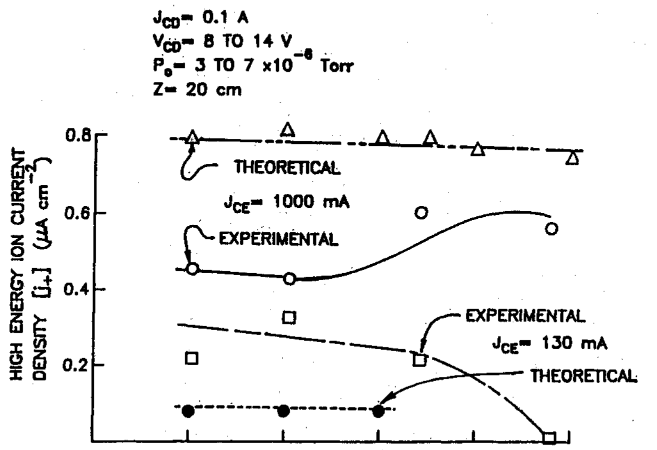

a) Ion current density

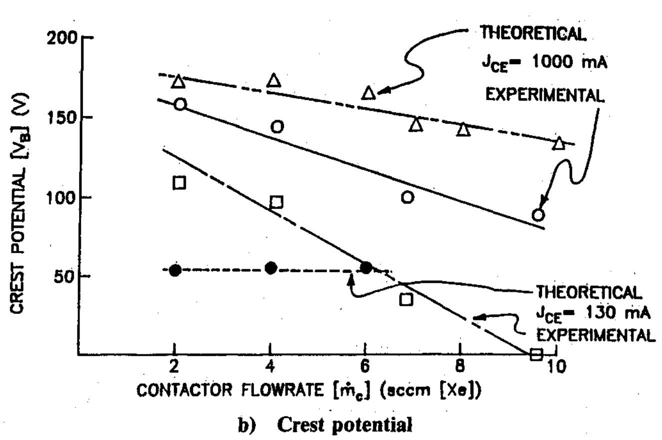

b) Crest potential

Fig. 11 Comparison of measured and computed effects of contactor flowrate.

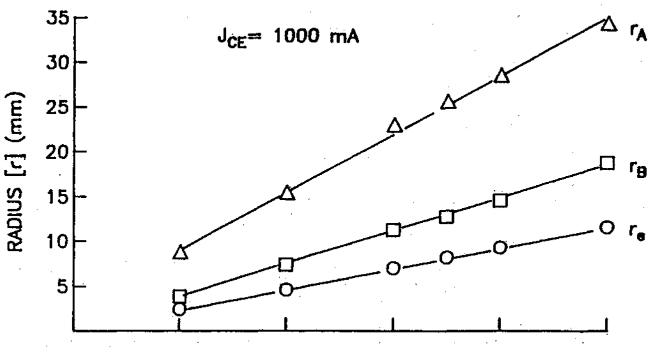

a) High electron emission current condition

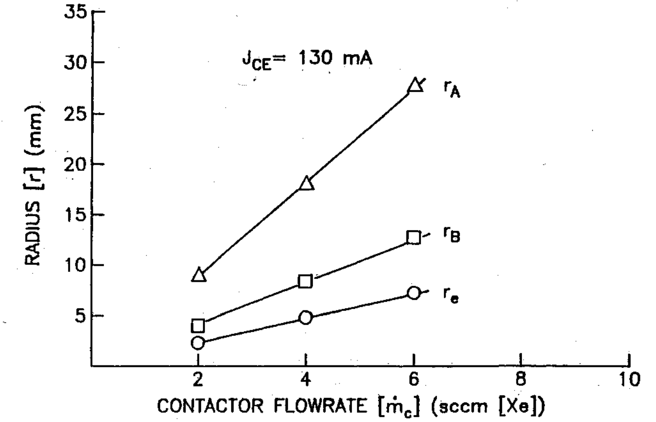

b) Low electron current condition

Fig. 12 Computed effects of contactor flowrate on the radii of electron source, crest and downstream boundaries.

indicate, at a contactor flowrate of 9.6 sccm, that no high-energy ions are present. At this high flowrate and low electron emission level, apparently no potential hill structure is needed to assist electron emission from the high-density plasma near the contactor hollow cathode. Convergent numerical solutions could not be obtained at the 130-mA condition at flowrates greater than 6 sccm unless the downstream potential V_A was artificially increased to ~ 14 V (from actual measured values of 8–12 V). Consequently, these data were not included on Fig. 11. The computed values of r_e, r_B, and r_A corresponding to Fig. 11 are shown in Fig. 12. In this figure, higher flowrates are shown to induce larger radii and these radii increase linearly with flowrate. It is noted that the trends shown in Fig. 11 could be dependent upon the contactor discharge current. At a contactor discharge current other than 100 mA, a different flowrate than the ~9.6 sccm value associated with the figure would be expected to eliminate the potential hill. The effects of discharge current were not investigated and are not included in the model because they are considered beyond the scope of this paper.

The agreement between the numerical and experimental results shown in Figs. 9 and 11 is considered to be good. In addition, the rate of ion production (expressed as a current) in the potential hill region is small compared to the electron emission current for all of the comparisons made in these figures. Hence, the rate of low-energy (secondary) electron production is also small and it should be possible to remove them as they are produced using a small fraction of the power in the streaming electron beam. Recall their removal via an undefined mechanism is assumed in the model. Several experimental observations have been made which suggest that fundamentally different phenomena occur at certain emission current and contactor flowrate condition ranges. For example, high emission current and/or low-flowrate operating conditions induce higher noise levels, higher anode voltages, and generation of energetic ions when compared to low emission current and/or high-flowrate operating conditions. At low emission currents and high-flowrate conditions, a small, relatively bright (luminous) spot is observed just downstream of the contactor orifice. Operation of a hollow cathode discharge under these conditions has been termed the "spot mode,"[8] and a potential hill is not present under these conditions. Conversely, at high emission currents or low flowrates, a rather large (several centimeters in extent) luminous region develops downstream of the contactor cathode. Operation of a hollow cathode under these conditions has been termed the "plume mode."[8] A majority of the experimental evidence presented here has been collected in the plume mode of operation, and the model has been developed to describe this operational mode. However, transitions from the plume to spot modes have been observed experimentally and the model has been seen to break down at conditions close to those where the transition occurs. It is possible that operation in the spot mode occurs at high flowrates when the neutral density is very high near the contactor orifice region because the electrons suffer many kinetic energy degrading collisions here and cannot acquire the streaming energies needed to induce substantial ionization and create a potential hill.

Conclusions

Experimental observations of a hollow cathode-based plasma contactor emitting electrons to a ambient plasma suggest that a potential hill structure develops close to the contactor cathode. It is postulated that the potential hill is created by a region of positive space charge, and ions produced in this region can gain substantial energies as they are accelerated away from the region. By measuring the energies of these ions, the height of the potential hill can be inferred. In general, an increase in contactor flowrate tends to reduce the potential at the crest of the hill, while larger emission current levels tend to increase it.

A simple model that reflects the effects of ionization, ion and electron acceleration, and the space-charge induced by the ions and electrons describes the essential features derived from experimental observations of hollow cathodes emitting electrons. Specifically, it yields magnitudes of potential hill height and current density of ions flowing from the potential hill that agree with experimental results. Furthermore, the predicted effects of electron emission current and contactor flowrate on these features agree with experimentally observed trends. It is noted that the total current of ions emitted to the expanding plasma is estimated to be small compared to the electron emission current (i.e., typically less than 0.2%). This suggests that only a small fraction of the electrons flowing from the contactor to the expanding plasma interact with and possibly ionize neutral atoms while they stream through the potential hill region.

References

[1] Williams, J. D., and Wilbur, P. J., "Experimental Study of Plasma Contactor Phenomena," *Journal of Spacecraft and Rockets*, Vol. 27, No. 6, 1990, pp. 634–641.

[2] Vannaroni, G., Cosmovici, C. B., McCoy, J., Bonifazi, C., Dobrowalny, M., Guidoni, U., Iess, L., and Scandurra, L., "Experimental Characterization of Hollow-Cathode Plasma Sources at Frascati," *Space Tethers for Science in the Space Station Era*, edited by L. Guerriero and I. Bekey, Societa Italiana Di Fisica, Vol. 14, Bologna, Italy, Oct. 1987, pp. 254–260.

[3] Patterson, M. J., and Aadland, R. S., "Ground-Based Plasma Contactor Characterization," *Space Tethers for Science in the Space Station Era*, edited by L. Guerriero and I. Bekey, Societa Italiana Di Fisica, Vol. 14, Bologna, Italy, Oct. 1987, pp. 261–268.

[4] Gerver, M. J., Hastings, D. E., and Oberhardt, M., "Theory of Plasma Contactors in Ground-Based Experiments and Low Earth Orbit," *Journal of Spacecraft and Rockets*, Vol. 27, No. 4, 1990, pp. 391–402.

[5] Katz, I., and Davis, V. A., "A Van der Waals-Like Theory of Plasma Double Layers," *Physics of Fluids*, Vol. B1, Oct. 1989, pp. 2121–2125.

[6] Davis, V., Katz, I., Mandell, M., and Parks, D., "A Model of Electron Collecting Plasma Contactors," *Journal of Spacecraft and Rockets,* Vol. 28, No. 3, 1991, pp. 292–300.

[7] Friedly, V. J., and Wilbur, P. J., "High Current Hollow Cathode Phenomena," AIAA Paper 90-2587, July 1990.

[8] Siegfried, D. E., and Wilbur, P. J., "A Model for Mercury Orificed Hollow Cathodes: Theory and Experiment," *AIAA Journal,* Vol. 22, No. 10, 1984, pp. 1405–1412.

[9] Davis, W. D., and Miller, H. C., "Analysis of Electrode Products Emitted by DC Arcs in a Vacuum Ambient," *Journal of Applied Physics,* Vol. 40, No. 3, 1969, pp. 2212–2221.

[10] Tanberg, R., "On the Cathode of an Arc Drawn in Vacuum," *Physical Review,* Vol. 35, May 1930, pp. 1080–1089.

[11] Brophy, J. R., and Wilbur, P. J., "An Experimental Investigation of Cusped Magnetic Field Discharge Chambers," International Electric Propulsion Conf., IEPC 84-70, Tokyo, July 1984.

[12] Williams, J. D., "Plasma Contactor Research," edited by P. J. Wilbur, NASA CR-185212, Feb. 1990, pp. 32–39.

[13] Aston, G., and Wilbur, P. J., "Ion Extraction from a Plasma," *Journal of Applied Physics,* Vol. 52, No. 4, 1981, pp. 2614–2626.

[14] Hershkowitz, N., "Review of Recent Laboratory Double Layer Experiments," *Space Science Reviews,* Vol. 41, No. 3–4, 1985, pp. 351–391.

[15] Anderson, J. R., "A Fourier Series Technique for Differentiating Experimental Data," Appendix C in NASA CR-182254, edited by P. J. Wilbur, Feb. 1989, pp. 67–79; see also Lanczos, C., *Applied Analysis,* Prentice Hall, Englewood Cliffs, NJ, 1964, pp. 219–221.

[16] Rapp, D., and Englander-Golden, P., "Total Cross Sections for Ionization and Attachment in Gases by Electron Impact. I. Positive Ionization," *Journal of Chemical Physics,* Vol. 34, No. 5, 1965, pp. 1464–1479.

Paul F. Mizera
Associate Editor